

# A REVIEW OF EARTH-BASED RADAR MAPPING OF THE MOON\*

T. W. THOMPSON

*Planetary Science Institute, Pasadena, Calif., U.S.A.*

(Received 7 September, 1978)

**Abstract.** Lunar radar mappings carried out in the late 1960's and 1970's have provided several valuable insights into lunar surface processes. These radar mappings used the delay-Doppler technique developed by Gordon Pettengill and his colleagues. These radar mappings also needed the narrow antenna beams, now available with large radio telescopes such as those at the Arecibo and Haystack Observatories. Two-element radar interferometers have provided resolution of the delay-Doppler ambiguity at meter wavelengths and provided topographic information at centimeter wavelengths. These techniques have provided high-resolution lunar radar-maps at 3.8-cm, 70-cm, and 7.5-m wavelengths, a set of wavelengths which span the window available for Earth-based radar mapping of the Moon.

These radar maps have been used along with other Earth-based and Apollo orbital measurements to define surface units. The radar maps and these other data can describe physical properties such as small-scale (centimeter sized) blockiness and surface chemistry (titanium and iron) content. These estimates of lunar surface properties rely heavily upon extrapolation of surface sampling results.

## 1. Introduction

The Moon was first detected by radar in 1946 when surplus military radars were directed toward the Moon (see Evans, 1962, for an excellent review of the early lunar radar measurements). In the 1960's Lincoln Laboratory developed powerful, sophisticated radars able to make detailed measurements of the Moon's average scattering behavior (see, for example, the reviews given by T. Hagfors, 1967 and 1970). Also in the 1960's, Gordon Pettengill and his colleagues developed the delay-Doppler radar mapping technique and detected strong radar echoes associated with the lunar crater Tycho (Pettengill and Henry, 1962). In the late 1960's and early 1970's, radars at the Arecibo and Haystack Observatories became operational and their narrow antenna beams permitted a straightforward resolution of the delay-Doppler ambiguity. Radar echoes from the Earth-visible lunar hemisphere have been mapped at 3.8-cm and 70-cm wavelengths (Zisk *et al.*, 1974; and Thompson, 1974, respectively). Also in the early 1970's, interferometry was combined with delay-Doppler technique for two important mapping experiments; the measurement of lunar heights described by Shapiro *et al.* (1972) and the mapping of radar echo strength at 7.5-m wavelength by Thompson (1970 and 1978).

Although this paper emphasizes the radar mapping results at 3.8 cm, 70-cm, and 7.5-m wavelengths, three other mapping experiments should be noted. The technique of aperture synthesis was adopted from radio astronomy and applied to lunar radar mapping by

\* Presented at the IAU-COSPAR Julian Schmidt Symposium on 100 Years of Lunar Mapping held at Lagonissi, Greece, 25-27 May, 1978.

Hagfors *et al.* (1968) and by Thomson and Ponsonby (1968). Also, a limited area of the Moon was mapped by the Apollo Lunar Sounder Experiment on-board the Apollo-17 Command Module (see Phillips *et al.*, 1973). The Lunar Orbiter and Apollo spacecraft also permitted mapping of large-scale surface roughness and surface slopes by a bistatic radar measurements, where radio emissions from the spacecraft were reflected off the Moon and received and recorded with Earth-based antennas (see Tyler and Howard, 1973). Results from these three experiments are not discussed in this article.

The maps of radar reflectivity produced in the early 1970's have provided new insights into physical and chemical properties of the lunar surface. Radar echo enhancements usually indicate increased surface roughness with meter and centimeter scales, sizes that are too small to be detected from orbit. Also, studies of radar and other data have shown that surface chemical composition can alter radar echo strength. Thus, radar echo strength can help delineate and characterize lunar surface units (Head *et al.*, 1978).

## 2. Techniques and Geometry

Gordon Pettengill and his colleagues at the Massachusetts Institute of Technology developed the delay-Doppler techniques in the 1960's and successfully detected enhanced radar echoes associated with the crater Tycho (Pettengill and Henry, 1962). This new technique led to observations at the Arecibo and Haystack Observatories, where the entire Earth-side lunar hemisphere was mapped with resolutions of 1 to 10 km. The geometry associated with this radar mapping technique will be discussed in this section.

Delay-Doppler radar mapping combines ranging and Doppler frequency resolution. Resolution in range is obtained by transmitting short pulses and by time-gating the echo. Resolution in Doppler frequency in other radar observations is usually obtained by transmitting a pure sine wave and by observing the frequency spectrum of the radar echoes. Resolution in Doppler frequency in delay-Doppler mapping is obtained by transmitting a string of pulses where the sine wave within any pulse is related to the sine waves in all other pulses. In particular, if the individual sine waves were extrapolated beyond the pulses they could form one continuous sine wave. The different Doppler shifts imparted by the Moon are then measured by sampling many consecutive pulses. This then allows simultaneous resolution of both the range and Doppler frequency, with a net result that radar echoes from small lunar areas can be isolated.

Let us now examine the geometry of delay-Doppler radar mapping. Two simplifying assumptions are made. First, the Moon is assumed to be a sphere with a radius of 1738 km; second, parallax is neglected. These assumptions, which introduce errors on the order of only a kilometer or two, are examined in greater detail by Pettengill *et al.* (1974). Figure 1 shows the relationship of radar echoes to the lunar surface, using a radar-based Cartesian coordinate system, centered on the Moon's center of mass. This coordinate system is convenient since constant delay contours lie in planes perpendicular to the Z-axis and constant Doppler-shift contours lie in planes perpendicular to the X-axis.

To visualize this radar-based coordinate system, imaging oneself positioned on the

**EARTH-BASED RADAR MAPPING OF THE MOON**

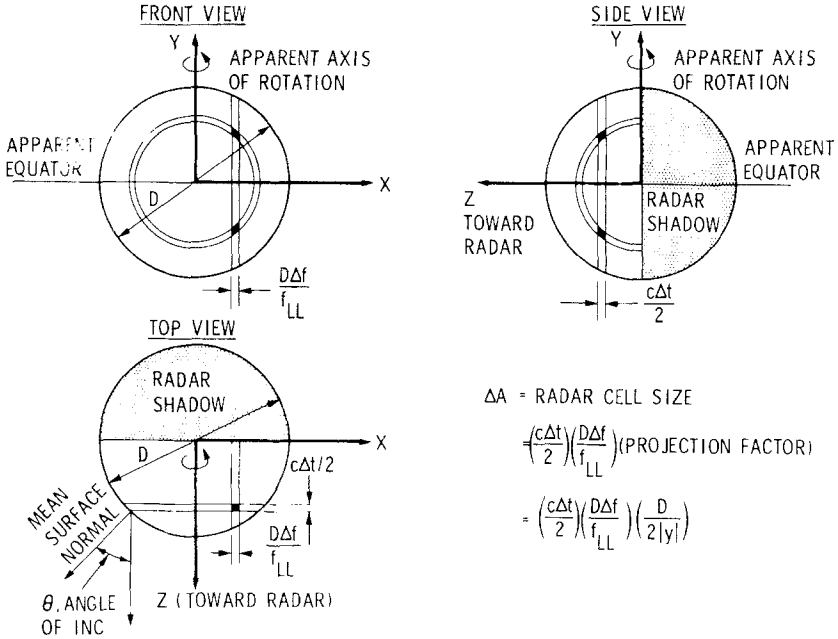


Fig. 1. Geometry for Earth-based mapping of the Moon. The front, top and side views of the Moon show the relationship between the delay and Doppler frequency rings and the radar-based X-Y-Z coordinate system. Also shown is radar cell size and angle of incidence,  $\theta$ .

lunar surface with the radar overhead. Your position is the subradar point, the intersection of the Z-axis, with the lunar surface. The subradar point moves across the lunar surface at a rate of a few kilometers per hour as dictated by the Moon's libration and the diurnal libration imparted by the Earth's rotation. Thus, the Moon slowly rotates in the radar-based coordinate system, such that the instantaneous velocity of the subradar point is along the X-axis. Radar astronomers use two terms – the apparent axis of rotation and apparent equator – which are tied to this X-Y-Z coordinate system. The apparent equator is the intersection of the X-Z plane with the lunar surface. The apparent axis of rotation is aligned with the Y-axis. The velocity of the subradar point is always along the apparent equator with a magnitude given by the product of lunar radius times the apparent rotation rate.

The first step in mapping radar echoes is to isolate echoes in range by measuring the time needed for the radar signals to travel to the Moon and back. This isolates the echo to a ring centered on the Z-axis. This ring, when viewed from the radar, is centered on the subradar point as shown in the front view of Figure 1. The ring in the top and side views of Figure 1 is viewed edge-on; and the edge-on width of this ring is  $(c\Delta t/2)$  where  $c$  is the velocity of light and  $\Delta t$  is the pulse width in time. Thus range resolution, the width of this ring on the surface, is  $[c\Delta t/2 \sin(\theta)]$  where  $\theta$  is the angle of incidence – the angle between the normal to the surface and the radar's line of sight.

The next step in mapping radar echoes is to determine the Doppler frequency of the echoes using a spectral analysis of many consecutive pulses. This determination of Doppler shift isolates the echoes to a second ring, which viewed from the radar appears as a strip parallel to the  $Y$ -axis. The projected width is  $(D\Delta f/f_{LL})$  where  $D$  is the Moon's diameter,  $\Delta f$  is the Doppler-frequency resolution of the measurement, and  $f_{LL}$  is the limb-to-limb Doppler-frequency difference across the Moon. The limb-to-limb frequency difference is also given by  $f_{LL} = 2\omega_a D/\lambda$  where  $\omega_a$  is the magnitude of the apparent rotation and  $\lambda$  is the radar wavelength. Thus the projected width is also given by  $(\Delta f\lambda/2\omega_a)$ . Radars with shorter wavelengths can obtain better resolutions with larger Doppler-frequency resolutions.

When these two steps are combined, the radar simultaneously resolves echoes in delay and Doppler frequency and the echoes come from small areas, the interactions of the two rings described above. In general, there are two intersections with the same delay and Doppler shifts, so something more is needed to assign echoes to only one area. Observations at 3.8-cm and 70-cm wavelengths have used antennas with small beams, so only one of these radar twins is illuminated by the main antenna beam. Differences in antenna gain between the main lobe and the side lobes assure that echoes from area illuminated by the main beam overpower the echoes from the twin areas illuminated by the side lobes. If all else is equal, the antenna provides an isolation of three or more orders of magnitude between areas that would have been equal otherwise. Thus, when the Arecibo and Haystack Observatories began observing with their small antenna beams, delay-Doppler mapping of the Moon became practical. The only drawback of this radar mapping technique is that only the areas illuminated by antenna beam can be mapped in a single observation. Thus, mapping of all the Earth facing portions of the Moon requires piecing many individual maps together into a mosaic.

Another radar technique, the combination of delay-Doppler processing with interferometry, also permits separation of echoes from the two areas with the same delay and Doppler. Radar echoes observed with two antennas, physically separated along a north-south baseline, are cross correlated producing sums and differences of powers from the two (otherwise ambiguous) areas. In addition, the combination of interferometry with small antenna beams permits measurement of lunar surface heights. The phase difference between echoes of the two antennae is directly related to the height of the echo area. See Thompson (1970), and Shapiro *et al.* (1974) for further details of these interferometer techniques.

Whether radar echoes are mapped by small antenna beams or with interferometers, the surface resolution can be defined by simple formulae. Range resolution when viewed edge-on is  $(c\Delta t/2)$ . Similarly, frequency resolution when viewed edge-on is  $(D\Delta f/f_{LL})$ . The top view of Figure 1 shows that the radar resolves an area whose projection is  $A = (c\Delta t/2)(D\Delta f/f_{LL})$ . Radar resolution on the surface is  $(A/|Y|)$  where  $|Y|$  is the magnitude of the distance between the reflecting area and the apparent equator. Thus, radar resolution can be expressed as a cell-size whose area varies over a mapped area. Also, most references to radar resolution refer to a length given by the square root of the resolved surface area described here.

In addition to isolating echoes to small areas, an essential part of radar mapping is the transformation of observed delays and Doppler shifts into selenographic coordinates of lunar latitude and longitude. The radar's measurement of range as described above assigns echoes to a ring, which can be assigned a single value of  $Z$  in a radar-based  $X$ - $Y$ - $Z$  coordinate system. In particular,

$$Z = 1 - (T/T_0).$$

The term  $T$  is the echo delay measured from the subradar point where the earliest echoes occur. The term  $T_0$  is the time delay between leading edge and limb echoes and is  $(D/c)$  or 11.595 milliseconds. Similarly, the measurement of Doppler shift by the radar assigns echoes to a value of  $X$ , given by

$$X = 2(f - f_0)/f_{LL},$$

where  $f$  = observed frequency of the echo and  $f_0$  is the Doppler frequency corresponding to the radial velocity for the Moon's center of mass. These two radar assignments combined with the assumption that the lunar surface is a sphere permits one to solve for the third radar-based coordinate, given by

$$Y = \pm (D^2 - X^2 - Z^2)^{1/2}.$$

The double sign for  $Y$  reflects the delay-Doppler ambiguity described above; the sign of  $Y$  is selected according to which area is illuminated by the antenna beam.

Once echo position can be defined in the radar-based  $X$ ,  $Y$ ,  $Z$  coordinate system shown in Figure 1, a straightforward transformation will convert these radar-based coordinates to selenographic coordinates. Rotation of the radar-based coordinates about  $Z$ -axis until the  $Y$ -axis lies in the plane of the central meridian realigns the radar-based coordinates into a coordinate system used for selenographic reductions from Earth-based photographs. Two additional rotations aligns these coordinates with the lunar equator and prime meridian. These transformations are based in large part on Cartesian coordinate transformation given by Arthur (1963), who used them to derive selenographic positions from Earth-based lunar photographs in an application similar to ours.

### 3. Polarization and Echo Strength Factors

In addition to resolving small areas on the lunar surface, other factors effect the radar maps. Polarization is important since radars have the ability to transmit carefully controlled polarization and receive echoes in opposite polarization. In addition, other manipulations remove echo variation inherent in the mapping caused by antenna gain variations across the main lobe and by the variation of cell size with delay and Doppler frequency.

Radar observations of the Moon are made with a polarized beam so that the depolarizing effects of the lunar surface could be studied. The Moon is illuminated with circularly polarized waves to eliminate Faraday rotation effects caused by the Earth's ionosphere. Radar echoes in the opposite sense of circular polarization are expected from mirror-like

reflections of flat areas oriented normal to the radar's line-of-sight. These are called the 'expected' or 'polarized' components of the echo. Radar echoes in the same sense of circular polarization are referred to as the 'depolarized' components of the echo. Thus, if right-hand circular polarization was transmitted, left-hand circularly polarized echoes would be the 'polarized component' and the right-hand circularly polarized echoes would be the 'depolarized component.'

It is convenient to display radar echo strengths with the display systems similar to those used for display spacecraft photography. Lunar radar echo maps contain many individual picture elements with digital intensities similar to values of light intensities obtained by spacecraft electronic imaging systems. Thus, television tubes are set up so that the horizontal and vertical position of spots corresponds to the mapped position of a map element. The intensity of a spot is controlled by the time the spot is left on the screen. The spots for stronger or weaker radar echoes are left on for longer or shorter times. The television screen is simply photographed to obtain a two-dimensional image corresponding to the radar map of the Moon. These displays are computer controlled so fiducial marks can be supplied and contouring can be performed in a straightforward manner.

Also, radar-echo displays generally remove several expected echo variations which can interfere with the interpretation of echo strength differences associated with lunar surface properties. A straightforward display of radar-echo strength would have three easily identifiable variations. First, the Moon has a natural scattering behavior that imparts a variation in echo strength of three orders of magnitude between the subradar point and the limb. Second, variation of the radar resolution cell-size on the lunar surface imparts a variation of about one order of magnitude across the mapped area. Third, the variation of the antenna gain across the mapped area imparts another variation of about one order of magnitude. The display of radar maps is enhanced by removing these predictable variations. The resulting display shows only departures from the average. The smallest differences discernible in the display correspond to echo differences of about ten percent. The largest scattering differences in a radar map vary from ten to one hundred times the average.

#### 4. Lunar Radar Mapping Results

The results presented here were obtained at radar wavelengths of 3.8-cm, 70-cm and 7.5-m. These three wavelengths span the window available for Earth-based observations shown in Figure 2. The 7.5-m wavelength is near the low frequency limit where the Earth's ionosphere limits the propagation of radio waves. The 3.8-cm wavelength is near the high frequency limit where absorption by the Earth's atmosphere limits observations. The 70-cm wavelength is nearly centered in this window. Radar parameters for these observations are given in Table I.

Figure 3 shows a lunar radar map at 7.5-m wavelength. This map has resolutions of 25 to 40-km and was obtained using delay-Doppler techniques combined with interferometry

TABLE I  
Parameters for Earth-based radar mapping of the Moon

Wavelength	7.5 m	70 cm	3.8 cm
Frequency	40 MHz	430 MHz	7840 MHz
Transmitter power	1.0 Mw	1.0 Mw	0.2 Mw
Transmitter pulse length	105 $\mu$ s	10–40 $\mu$ s	3–10 $\mu$ s
Range resolution	15–30 km	5–10 km	1–3 km
Spectral resolution	0.1 Hz	0.02 Hz	0.05 Hz
Coherent integration period	100 s	50 s	20 s
Spectra summed	82	25–50	80–90
Surface resolution	30–60 km	5–10 km	1–3 km
Antenna beam size	2° (120')	10'	4'
Antenna size	330 m	330 m	40 m
Observatory	Arecibo	Arecibo	Haystack
Reference	Thompson (1978)	Thompson (1974)	Zisk <i>et al.</i> (1974)

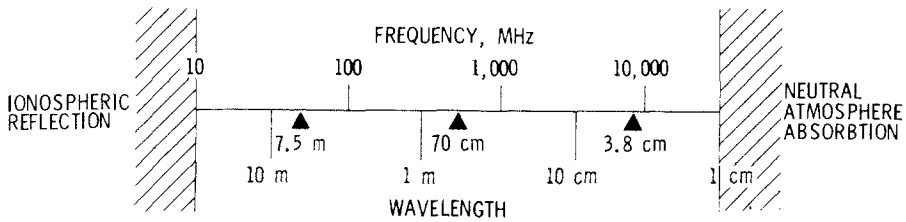


Fig. 2. The window for radio wave propagation through the Earth's atmosphere and ionosphere. Wavelengths longer than 30 m (frequencies less than 10 MHz) are reflected by charged particles in the Earth's ionosphere. Wavelengths shorter than about 1 cm (frequencies higher than 30 GHz) are absorbed by water and oxygen in the Earth's atmosphere. For more detail see Roger and Evans (1968). Triangles denote wavelengths used for the radar maps shown in Figures 3, 4, 5 and 9.

(Thompson, 1978). Although the resolution for this map was relatively coarse, as determined by ionospheric scintillations and signal-to-noise considerations, this map shows a consistent scattering difference between mare and terra. The maria and terrae have a similar scattering dependence on angle of incidence, but the maria backscatter less power than the terrae by factors of one-half to one-quarter. Backscatter enhancements associated with craters are seen, but are generally smaller than enhancements at shorter meter and centimeter wavelengths. This radar map has an artifact, a black strip running from northwest to southeast representing areas which could not be mapped by the radar interferometer. This area is along the apparent equator, where the two areas with the same delay and Doppler frequency have a small physical separation. This small separation creates a phase difference between the two antennas which is too small to be reliably measured. Also these areas have poor resolution since they have small values of  $Y$ . Much

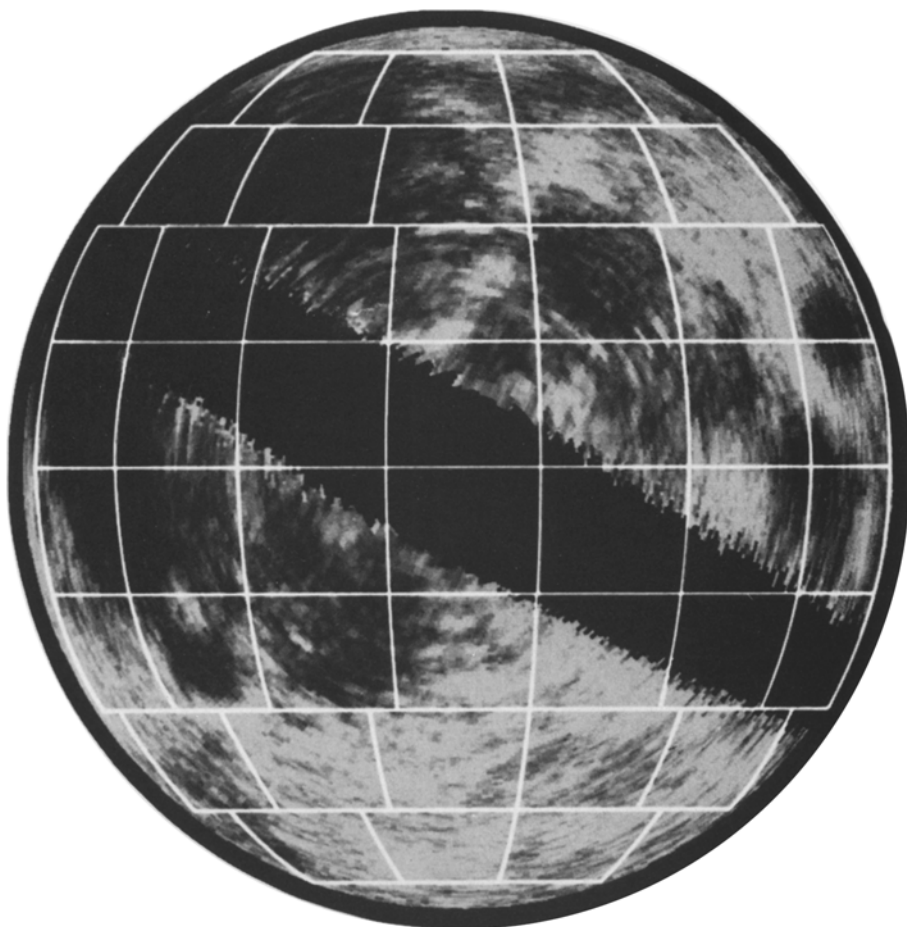


Fig. 3. Map of polarized 7.5-m radar backscatter from the Moon. Whiter areas have higher backscatter, darker areas have lower backscatter. Grid lines show LAC Chart boundaries as in Figures 4 through 8. This orthographic projection shows the Moon at mean libration. Black strip at limb is area where data was not taken because of low echo strength; black strip running from upper left to lower right (northwest to southeast) is area where echoes cannot be mapped. Radar resolution is 25–40 km.

of the missing area could be filled in by observations at some other time when the apparent equator would have a different tilt with respect to the true equator.

Figures 4 and 5 show the polarized and depolarized radar map at 70 cm wavelength (Thompson, 1974). This map has a resolution of 5 to 10 km and was obtained using the large radio telescope at Arecibo. This antenna has a beamwidth of ten minutes of arc, permitting resolution of the delay-Doppler ambiguity by pointing the antenna at the area of interest. Thus, a mapping strategy was adopted where individual areas were mapped on different days and these individual maps were to form the mosaics shown in Figures 2 and 3. Individual maps were tied to the Lunar Aeronautical Chart (LAC) Series, since LAC



Fig. 4. A mosaic of polarized lunar radar maps at 70-cm wavelength. The Moon is shown at mean libration and individual maps (corresponding to LAC Charts) are outlined. Radar echoes are normalized to show departures from the average; resolution is 5–10 km. See Figures 6, 7 and 8 for comparison with Earth-based optical and infrared observations.

Chart areas matched the data taking and processing facilities available then at the Arecibo Observatory. Map-to-map calibrations were not available so individual maps were arbitrarily adjusted to have a common average. Thus, the prominent mare-terra differences in the 7.5 m map do not appear in the 70 cm mosaic. However, earlier 70-cm measurements by Thompson and Dyce (1967) suggest that there are similar differences between mare and terra at both 7.5-m and 70-cm wavelengths.

Although the 70-cm radar map mosaic does not adequately display mare-terra differences over the lunar disk, the finer resolution of the 70-cm maps shows many enhancements associated with craters. The strongest enhancements are associated with the larger rayed craters such as Aristarchus, Copernicus, Langrenus, Kepler, Theophilus, and Tycho.



Fig. 5. A mosaic of depolarized lunar radar maps at 70-cm wavelength. The Moon is shown at mean libration and individual maps (corresponding to LAC Charts) are outlined. Radar echoes are normalized to show departures from the average; resolution is 5–10 km. See Figures 6, 7 and 8 for comparison with Earth-based optical and infrared observations.

Many other craters have enhancements, including craters as old as Plato and Gassendi, which are pre-mare in age. More details of these 70-cm radar maps is given in Thompson (1974). Figures 6, 7 and 8 are Earth-based optical photographs and infrared-eclipse temperature maps of the Moon for comparison with the radar maps given in Figures 3, 4 and 5.

Figure 9 shows a representative radar map at 3.8-cm wavelength (Zisk *et al.*, 1974). This 3.8-cm radar map was obtained using the small (four arc-minute) antenna beam to resolve the delay-Doppler technique. Radar resolution was 1 to 3 km, determined by both range and Doppler frequency resolutions combined with data processing considerations. Whereas some fifty beam positions could map the Earth-side hemisphere at

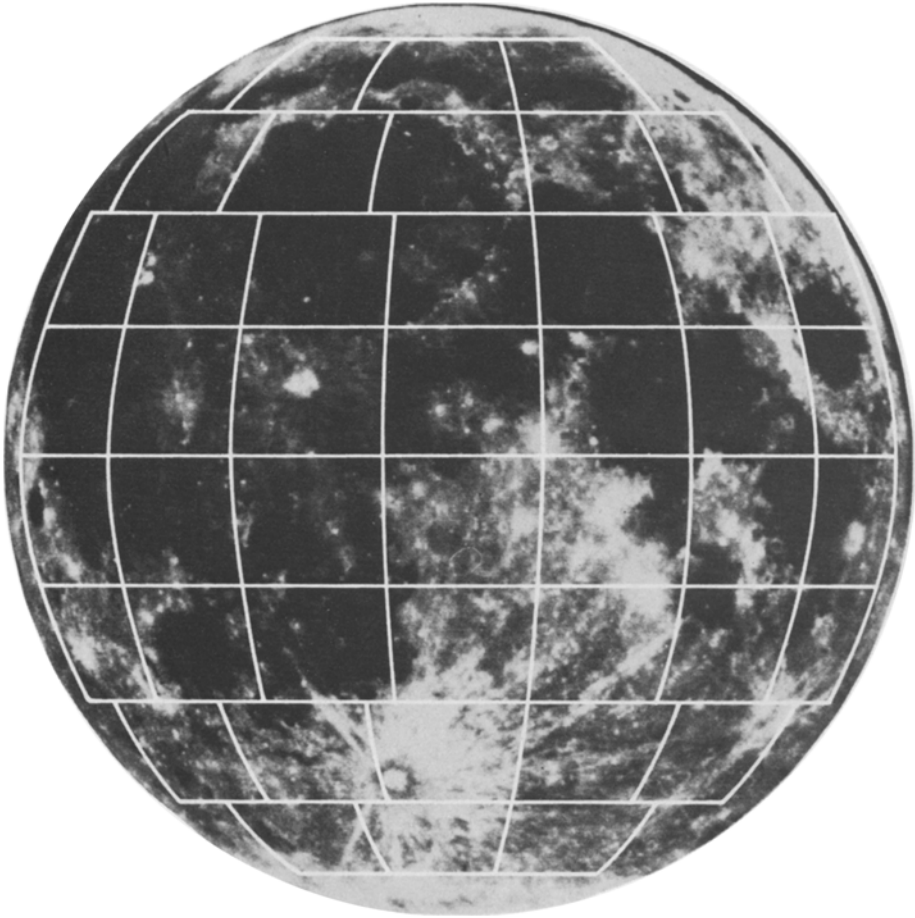


Fig. 6. Full Moon photograph for comparison of lunar features in the 7.5-m and 70-cm radar maps of Figures 3, 4 and 5.

70-cm wavelengths, some two hundred positions were required at 3.8-cm wavelength. Figures 10 and 11 show Earth-based photographs of the area shown in the 3.8 cm radar map of Figure 9.

The radar facilities at the Haystack Observatory have been supplemented with a second antenna, which forms a two-element interferometer that measures topography as well as backscatter. The measurement technique is described by Shapiro *et al.* (1972). The horizontal resolution remains 1 to 3 km, while height resolution is ten to a hundred meters, depending upon terrain. Individual map areas are restricted to areas illuminated by the antenna beam (i.e., to areas comparable to that shown in Figure 9). Individual maps can be pieced together to form mosaics of large areas (see, for example, the topographic map of Mare Crisium given by Zisk, 1978).

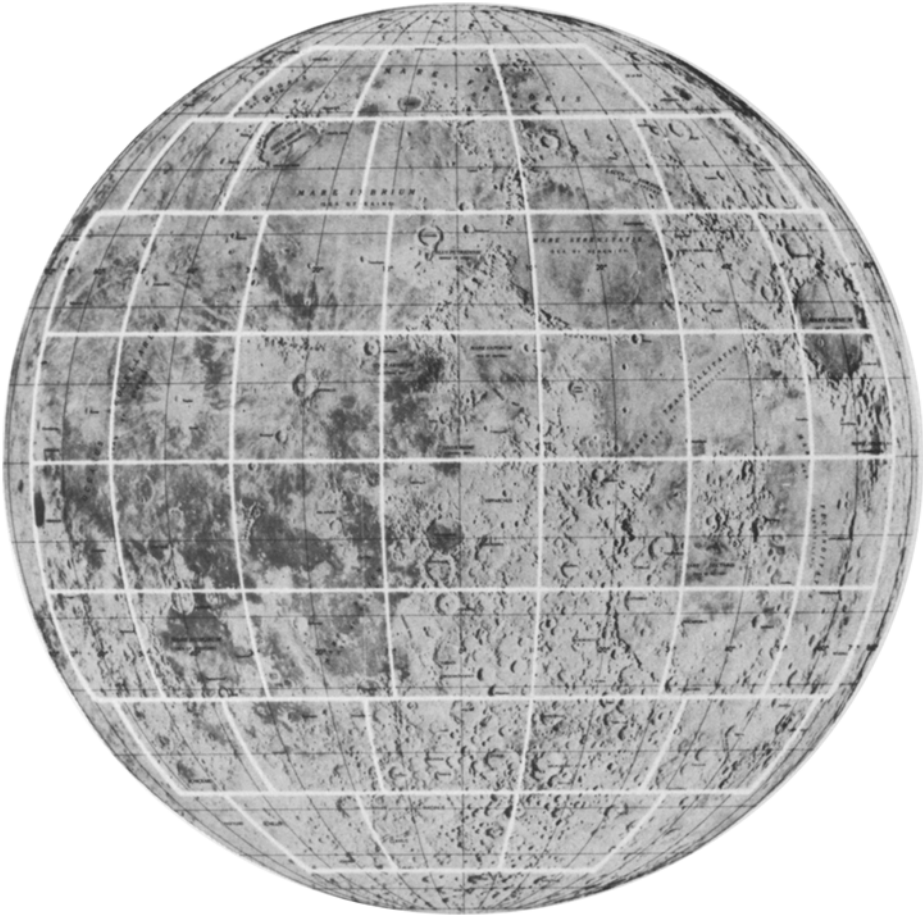


Fig. 7. Mosaic of low sun angle photographs for comparison of lunar features in the radar maps of Figures 3, 4 and 5.

### 5. Interpretation of Lunar Radar Maps and Earth-Based Observations

The lunar radar maps represented by the data given in Figures 3, 4, 5 and 9 provides a valuable data base of comparison with data at infrared and optical wavelengths. Head *et al.* (1978) and several studies described below, show that Earth-based radar maps can help identify and characterize lunar surface units.

Interpretation of lunar radar maps is based on theories derived from the Moon's average scattering behavior. Studies in the 1960's established that lunar radar backscatter had two components – diffuse and quasi-specular components (Evans and Hagfors, 1964; Thompson and Zisk, 1972; Pollack and Whitehill, 1972). Interpretation of lunar radar maps showed that backscatter was controlled by two factors – changes in the relative amount of diffuse components and tilts. Areas tilted toward or away from the radar

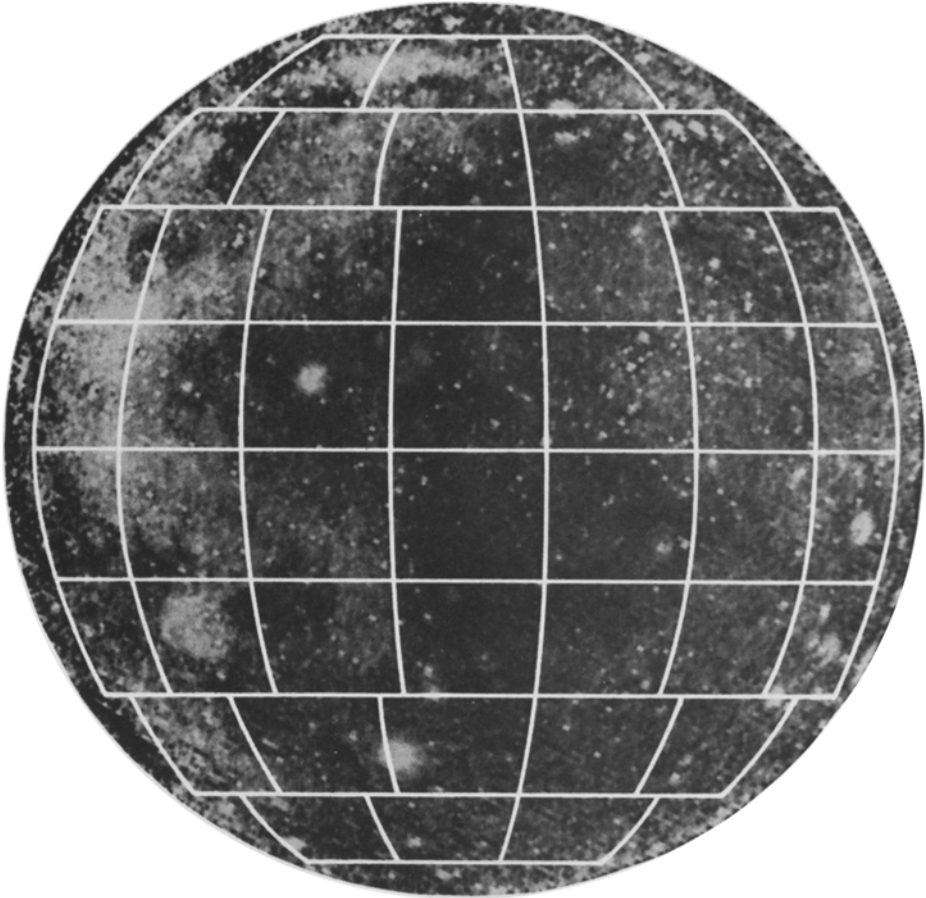


Fig. 8. Infrared eclipse temperature map of the Moon for comparison with the radar maps of Figures 3, 4 and 5. Data from Shorthill (1973).

would have stronger or weaker echoes for the simple reason that natural surfaces exhibit scattering behaviors where echo strength decreases monotonically with angle of incidence. Diffuse scattering is controlled by wavelength-size roughness arising from surface and near surface rocks.

The more important radar scattering differences appear where tilts cannot account for scattering differences. Here, changes in echo strength appear on level areas and are controlled by the relative amounts of diffuse and quasi-specular scattering. For example, most radar scattering enhancements associated with craters are associated with wavelength-sized debris created by impact cratering. Elsewhere, diffuse scattering from rocks buried in the regolith appears to be controlled by electrical losses associated with iron and titanium. Radar echo strength does not appear to be modulated by bulk dielectric constant since the Moon is covered by a regolith – a layer of debris where the bulk electrical

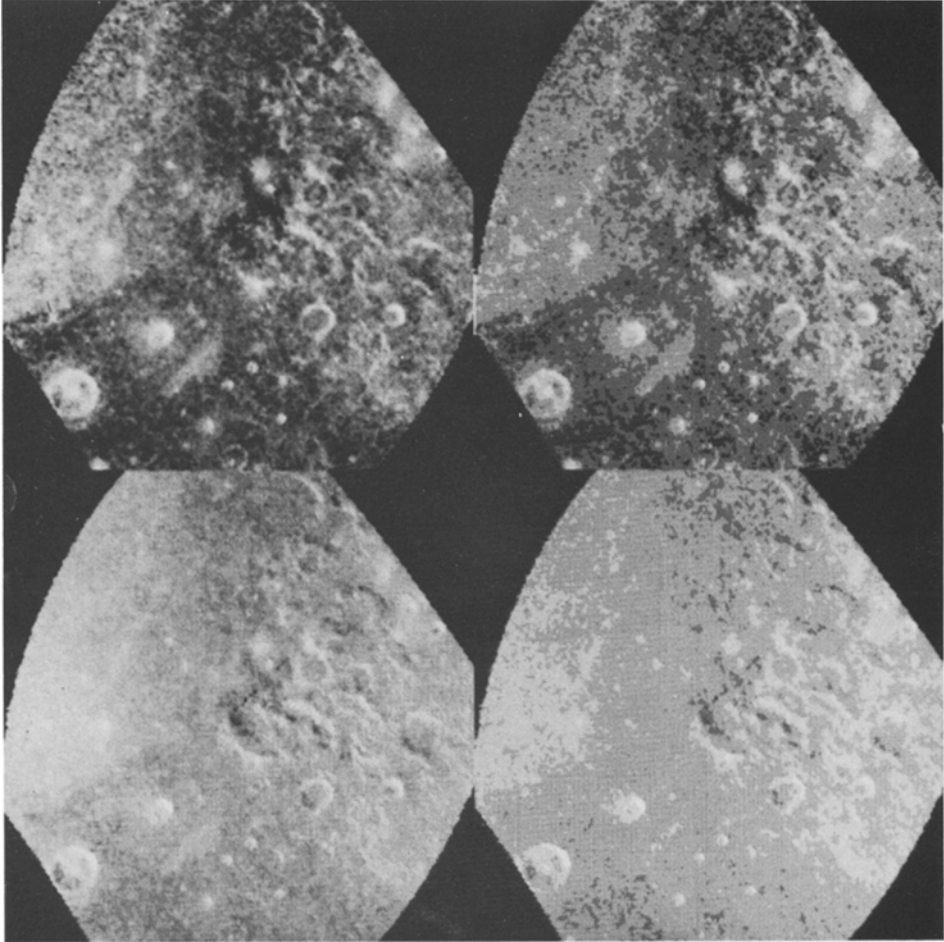


Fig. 9. 3.8-cm radar map of the Apollo-17 landing site and its environs. Center is  $30^{\circ}$  E,  $21^{\circ}$  N; image width is approximately 450 km; resolution is 1–3 km. Top frames show depolarized echoes; bottom frames show polarized echoes. Left-hand frames are continuous tone renditions; right-hand frames are quantized to levels which differ by a factor of two.

properties are determined primarily by the compaction of the debris. Thompson and Dyce (1967) and Thompson (1974) show that changes in dielectric constant do not provide good models for observed 70-cm backscatter differences. Also, Gold *et al.* (1976) and Campbell and Ulrichs (1969) show that theoretical models for the electrical models of pulverized rock dusts provide reasonable dielectric constants for the lunar surface.

Much of today's interpretation of lunar radar maps is based upon several studies in the 1970's which compared radar map data with data at optical and infrared wavelengths. These studies suggested that radar backscatter was correlated with lunar surface chemical composition; particularly iron and titanium contents. Measurement of the electrical and



Fig. 10. Earth-based low-sun photograph of the Apollo-17 landing site and its environs. Taken from Plate CII of *Consolidated Lunar Atlas* (Kuiper *et al.*, 1966).

optical properties of Apollo samples by Gold *et al.* (1976) showed that higher iron and titanium contents produce higher losses which absorb echoes from near surface rocks.

An early multiwavelength study by Thompson *et al.* (1974) considered the radar, infrared and geologic mapping of fifty-one craters. They showed that the higher radar backscatter and warmer lunar eclipse temperatures of young craters are consistent with the geologic interpretation that these young craters are blocky and largely unmodified by subsequent micrometeorite bombardment. Older craters had only longer wavelength radar enhancements and the oldest (terrae) craters had no enhancements at all. This study found a previously unknown feature – a halo of only centimeter-sized debris surrounding some intermediate (1–15 km) sized impact craters. This feature was characterized by



Fig. 11. Earth-based low sun photograph of the Apollo-17 landing site and its environs. Taken from Plate C5 of *Consolidated Lunar Atlas* (Kuiper *et al.*, 1967).

strong 3.8 cm radar enhancements accompanied by little or no enhanced 70-cm radar echoes and warmer eclipse temperatures.

Other multiwavelength studies have shown that radar echo strength combined with infrared and optical spectral data can characterize mare units. A study of Mare Serenitatis by Thompson *et al.* (1973) identified five surface types which correlate well with geologic units defined from interpretation of Apollo orbital photography (Howard *et al.*, 1973).

Figure 12 shows optical and 70-cm radar data for Mare Serenitatis along with a sketch map of surface types. Surface type II, which occurs in west central Mare Serenitatis, is visible only in the radar and color-difference data. The radar and other responses indicate that differences in surface chemical composition are a reasonable explanation for the observations shown in Figure 12.

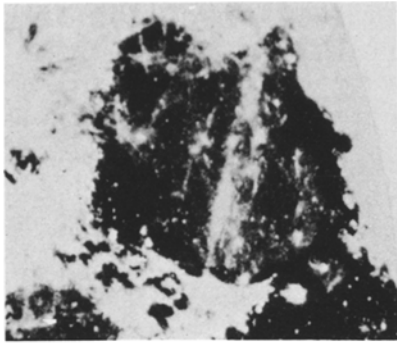
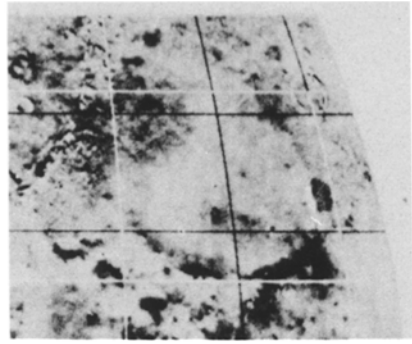
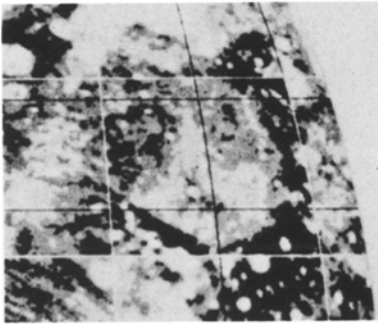
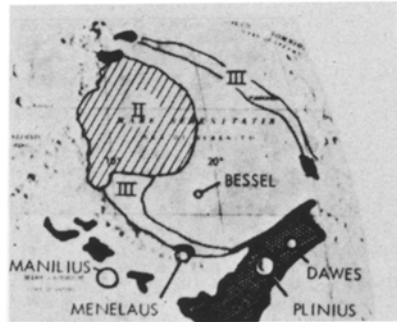
**FULL MOON PHOTO****COLOR-DIFF. PHOTO****70cm RADAR MAP****SURFACE TYPES**

Fig. 12. Multiwavelength data and surface-type sketch map of Mare Serenitatis. Area shown is bounded by latitudes  $10^{\circ}$  N and  $40^{\circ}$ , longitudes  $0^{\circ}$  E and  $35^{\circ}$  E. Taken from Thompson *et al.* (1973). Color difference photography from Whitaker (1972).

Schaber *et al.* (1975) showed that the Earth-based 3.8-cm and 70-cm radar echoes from Mare Imbrium are related to the color and age of mare units. Furthermore, Schaber *et al.* (1973) suggest that the reduction of radar backscatter from red to blue mare surfaces can be attributed to increased titanium and iron contents from ilmenite ( $\text{FeTiO}_3$ ).

Pieters *et al.* (1973) showed that low 3.8-cm radar echo strength associated with low optical albedos and distinct optical spectral types form a distinct lunar surface type, a mantle of ash or cinder with high iron and titanium contents. This distinct surface type is found at the Sulpicius Gallus formation and at the Apollo-17 landing site. Pieters *et al.* (1975) also studied the Mare Humorum area and used 3.8 cm radar backscatter and topographic measurements to define nine distinct mare surface units, based upon surface chemical compositions and other factors.

The Aristarchus Plateau provided another area where Earth-based radar was combined

with other remotely sensed data such as infrared eclipse temperature maps, color difference photography and Apollo photographic and orbital geochemical data. The study of the Aristarchus Plateau by Zisk *et al.* (1977) indicated that the Aristarchus Plateau is probably mantled up to depths of 50 to 300 m by a pyro-clastic material, which is fine grained with relatively few blocks greater than 10 cm. The physical and chemical characteristics of this mantle material resemble the orange glass beads found at Shorty crater during the Apollo-17 mission. Photo-interpretation of Apollo orbital photography indicated that this Aristarchus Plateau mantle was deposited before the nearby mare units were emplaced. One of the striking results of the Aristarchus Plateau study is that Earth-based observations combined with Apollo orbital data provided a meaningful interpretation of a region some 2400 km away from the Apollo-17 landing site where the orange glasses were found.

In addition to backscatter maps, the Earth-based radar topography have provided insights into lunar surface characteristics. A recent study of Mare Crisium by Adams *et al.* (1978) used Earth-based radar topographic data to characterize surface units. The topographic data helped define a history where the Mare Crisium basin was filled by different episodes of mare filling interweaved with extensive warping and downfaulting of the inner part of the basin.

## 6. Future Studies

Earth-based radar mapping of the Moon has followed a progression of improvements starting with surplus World War-II radars to the sophisticated radars at the Arecibo and Haystack Observatories. A number of improved radar observations can be envisioned. A depolarized radar map of the Moon at 7.5-m wavelength, would help distinguish whether the mare-terrae differences at meter wavelength is caused by differences in diffuse or quasi-specular scattering (see Thompson, 1978). Also, new radar maps at 70-cm wavelength with resolutions of 1–3 km is now possible with upgraded data acquisition at the Arecibo Observatory. The mare-terra scattering differences so evident in the 7.5-m map should be investigated further at the other radar wavelengths.

In addition to improving the observations, theoretical studies are needed for better understanding of radar backscatter. Sophisticated optical scattering models for the scattering of light from planetary atmospheres may provide useful analogs to the radar problem.

## Acknowledgements

Radar mapping projects at the Haystack and Arecibo Observatory were carried out with funding support from the National Aeronautics and Space Administration (NASA) and with day-to-day support of the observatory staffs. The multiwavelength studies have been funded by various programs under the Lunar and Planetary Programs area of NASA. Apollo Experiment S-217 (IR/Radar Study of Apollo Data) and Apollo Experiment S-222 (Photogeology) provided an important base for many of the multiwavelength

studies involving the 70 cm radar maps. Many radar map displays under Apollo Experiment S-217 were done using the facilities of the Image Processing Laboratory at the Jet Propulsion Laboratory.

The Arecibo Observatory is part of the National Astronomy and Ionospheric Center, which is operated under contract with the National Science Foundation. Work performed at the Jet Propulsion Laboratory, California Institute of Technology, represents one phase of the research sponsored by the National Aeronautics and Space Agency under Contract NAS7-100.

### References

- Adams, J. B. *et al.*: 1978, *Geophys. Res. Letters* **5**, 313–316.
- Arthur, D. W. G.: 1963, in *Moon, Meteorites and Comets*, vol. IV of *The Solar System*, Univ. of Chicago Press, Chicago, pp. 55–77.
- Campbell, M. J. and Ulrichs, J.: 1969, *J. Geophys. Res.* **74**, 5867–5881.
- Evans, J. V.: 1962, Chapt. 12 in Z. Kopal (ed.), *Physics and Astronomy of the Moon* Academic Press, London pp. 429–479.
- Evans, J. V. and Hagfors, T.: 1964, *Icarus* **3**, 151–160.
- Gold, T. *et al.*: 1976, *Proc. Lunar Sci. Conf. 7th (Geochimica et Cosmochimica Acta, Suppl. 7)*, 2593–2603.
- Hagfors, T.: 1967, *Radio Sci.* **2** (new series) 445–465.
- Hagfors, T.: 1970, *Radio Sci.* **5**, 189–227.
- Hagfors, T. *et al.*: 1968, *Radio Sci.* **3**, 491–508.
- Head, J. W. *et al.*: 1978, *Icarus* **33**, 45–72.
- Howard, K. A. *et al.*: 1973, 'Basalt Stratigraphy of Southern Mare Serenitatis', part A, Chapt. 29 in *Apollo 17 Prel. Science Report*, NASA SP-33, (pp. 29–1 to 29–13).
- Kuiper, G. P. *et al.*: 1967, *Consolidated Lunar Atlas*, Supplement and 4 of *USAF Photographic Lunar Atlas*; Lunar and Planetary Lab., Univ. of Arizona, Tucson, AZ.
- Pettengill, G. H. and Henry, J. C.: 1962, *J. Geophys. Res.* **67**, 4881–4885.
- Pettengill, G. H. and Thompson, T. W.: 1968, *Icarus* **8**, 457–471.
- Pettengill, G. H. *et al.*: 1974, *The Moon* **10**, 1–16.
- Phillips, R. J. *et al.*: 1973, *Apollo 17 Prel. Sci. Report* (NASA SP-330, Wash. D.C.), Chapt. 22, 1–26.
- Pieters, C. *et al.*: 1973, *J. Geophys. Res.* **78**, 5867–5875.
- Pieters, C. *et al.*: 1975, *Proc. Sixth Lunar Sci. Conf., Geochem. Cosmochem. Acta*, 2689–2710.
- Pollack, J. B. and Whitehill, L.: 1972, *J. Geophys. Res.* **77**, 4289–4303.
- Rogers, T. F. and Evans, J.: 1968, Chapt. 2 in J. V. Evans and T. Hagfors, (eds.), *Radar Astronomy*, McGraw-Hill, New York.
- Schaber, G. G. *et al.*: 1975, *The Moon* **13**, 395–423.
- Shapiro, I. I. *et al.*: 1972, *Science* **178**, 939–948.
- Shorthill, R. W.: 1973, *The Moon* **7**, 22–45.
- Thompson, T. W.: 1970, *Icarus* **13**, 363–370.
- Thompson, T. W.: 1974, *The Moon* **10**, 51–85.
- Thompson, T. W.: 1978, 'High Resolution Lunar Radar Map at 7.5 Meter Wavelength', *Icarus* **36**, 174–188.
- Thompson, T. W. and Dyce, R. B.: 1965, *J. Geophys. Res.* **71**, 4843–4853.
- Thompson, T. W. and Zisk, S. H.: 1972, Chapt. 1c in *Thermal Characteristics of the Moon*, Vol. 28 of *Progress in Aeronautics and Astronautics*, MIT Press, Cambridge, Mass., pp. 83–117.
- Thompson, T. W. *et al.*: 1970, *Radio Sci.* **5**, 253–262.
- Thompson, T. W. *et al.*: 1974, *The Moon* **9**, 89–96.
- Thompson, T. W. *et al.*: 1973, 'Remote Sensing of Mare Serenitatis', part A, Chapt. 33 in *Apollo 17 Prel. Sci. Report*, NASA SP-330 (pp. 33–3 to 33–10).

- Thompson, T. W. *et al.*: 1974, *The Moon* **10**, 87–117.
- Thompson, J. H. and Ponsonby, J. E. B.: 1968, *Proc. Roy. Soc. London* **A303**, 477–491.
- Tyler, G. L. and Howard, H. T.: 1973, *J. Geophys. Res.* **78**, 4852–4874.
- Whitaker, E. A.: 1972, *The Moon* **4**, 523–530.
- Zisk, S. H.: 1978, 'Mare Crisium Area Topography: A Comparison of Earth-Based Radar and Apollo Mapping Camera Results', accepted for publication in *Mare Crisium: The View From Luna 24*.
- Zisk, S. H. *et al.*: 1974, *The Moon* **10**, 17–50.
- Zisk, S. H. *et al.*: 1977, *The Moon* **17**, 59–99.